Design of the 1 MeV D^- SINGAP accelerator for ITER neutral beam injection

H.P.L. de Esch, R.S. Hemsworth, P. Massmann
Association Euratom-CEA, CEA Cadarache, F-13108 St. Paul-lez-Durance CEDEX, France

This paper (except section 7) has been submitted to Fusion Engineering and Design

Abstract: In contrast to the Multi Aperture – Multi Grid (MAMuG) concept of the ITER Neutral Beam Injector reference design (Inoue *et al.* [1]) in which D^- acceleration to 40 A, 1 MeV is achieved through 7 grids containing 1280 apertures each, the European SINGAP (SINgle GAP - SINGle APerture) concept proposes acceleration of 1280 pre-accelerated (20-50 keV) beamlets to 1 MeV in a single step. During acceleration the beamlets are merged into 16 beam groups of 80 beamlets. These 16 beam groups ("hyperbeamlets") then emerge from an exit grid containing only 16 very large apertures. This concept is expected to reduce cost and increase the tolerance to mechanical errors and stray magnetic fields. The physics of this concept and a design have been described before by ourselves [2]. Improved computational facilities have enabled us to calculate larger models and this has led to necessary modifications to the design which are described in this paper.

Keywords: Neutral beam injection, Negative ions, SINGAP, Beam optics

1. Introduction

Two (possibly three) 1 MeV, 17 MW neutral beam injectors based on negative ions have been proposed for International Tokamak Experimental Reactor (ITER). Beamlets are extracted from a plasma source using multi-aperture grids containing 1280 apertures. Subsequently, the extracted beamlets are accelerated to 1 MeV. The apertures in the plasma and extraction grids are arranged in 16 rectangular groups of 5x16 apertures (horizontal x vertical). These groups form 4 columns each containing 4 groups [1]. The accelerator then produces 4 "column beams" which allow the neutraliser to be subdivided. This is necessary to reduce the neutraliser conductance, hence the gas flow, and to keep the beamline short. The residual ion dump (RID), which is located downstream of the neutraliser, consists of 5 parallel plates forming the channels in line with the neutraliser channels. Ions are deflected onto the plates by an electric field created by polarising alternate plates. The overall result is a compact beamline and low power density on the RID. The downside is that the resulting geometry in the horizontal direction is restrictive, which necessitates good beam steering and low beamlet divergence in order to have good beam transmission.

To obtain the high-energy neutral beams two accelerator concepts are considered.

- The reference concept, the "**M**ulti **A**perture **MU**lti **G**rid" ("MAMuG") accelerator, accelerates the ions to high voltage in several intermediate steps, each having the same aperture pattern as the plasma and extraction grids. This requires several multi aperture grids at intermediate potentials, the power supplies to feed them and water cooling to each grid.
- The European alternative concept, the **SING**le **A**perture – **SIN**gle **GAP** (SINGAP) accelerator, pre-accelerates the 1280 beamlets to 20-50 keV, then accelerates to the final energy in one single step through 16 large apertures in the final (ground potential) electrode. These 16 'hyperapertures' correspond to the 4x4 sections in the pre-accelerator.

Figure 1 shows a sketch of both concepts. The beamline design is described by Inoue *et al.* [1]. A very detailed description is available in the ITER DDD 5.3 [3] which is, unfortunately, not easily accessible to everybody.

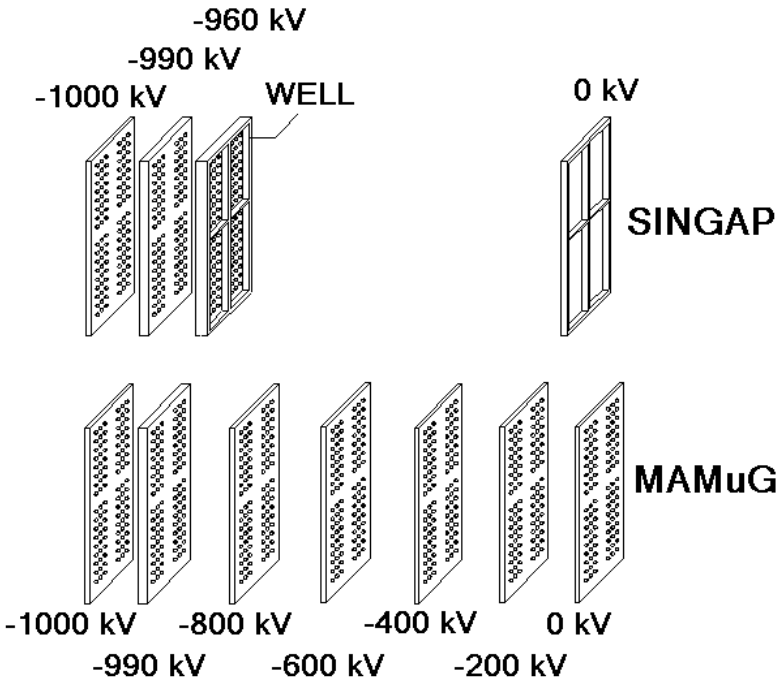

Figure 1: *A sketch of ¼ of the SINGAP and MAMuG negative ion accelerators for ITER.*

We presented a physics design for SINGAP before [2]. Computational limitations meant that only ¼ of a single beam group could be simulated. Symmetry was used to infer the rest, which is only an approximation as there are not an infinite number of beam groups. In this paper simulations are presented that model ¼ of the *entire* accelerator inside its vacuum vessel. Although the optics of the individual beamlets was lost, the behaviour of the system as a whole could be modelled in much more detail. It was found that:

- Structures bolted *on* the pre-acceleration grid ("kerbs") have to be replaced by structures sunk *in* the grid ("wells"). This means that the pre-acceleration grid as a whole becomes much thicker, except where the beam groups emerge.
- Structures bolted *on* the post-acceleration grid (the SINGAP electrode) can be used to steer the beams horizontally. Only very slight aperture-offset needs to be provided to optimise the beam steering. These kerbs also help counteract the space-charge repulsion between the beamlets.
- Making the post-acceleration grid slightly "V"-shaped (with the tip of the "V" to the upstream side) allows vertical steering of the beams.
- One (very large) aperture in the post-acceleration grid distorts the potential of its neighbours. The effect of this is included in the simulations.

Eliminating the need to use aperture-offset steering for the beam alignment allows the grounded grid (with the wide apertures) to be moved vertically in order to steer the beams between "on-axis beams" and "off-axis beams" positions [1]. This eliminates the need for a tilting mechanism for the source and accelerator, which are heavy (26 tonnes), with many components at high potential.

Further modelling work (since 2002 [2]) on the extractor and pre-accelerator led to a modified shape of the extraction grid. This enabled us to reduce the extraction gap from 5 to 3 mm and the extraction voltage from 9 kV to 6 kV, leading to reduced power from co-extracted electrons on the extraction grid. The energy of the pre-accelerated beamlets is increased from 34 to 40 keV.

2. SINGAP beam optics

Three space charge effects occur when accelerating 16 groups of 5x16 beamlets.

1) Electrostatic repulsion between the individual beamlets. In MAMuG the effect is strongly reduced by the intermediate grids. In SINGAP this effect is counteracted by fitting a material structure (a "kerb" or "well") around each beam group to the downstream side of the pre-accelerator (see fig. 2b).
2) Electrostatic repulsion inside each individual beamlet. In MAMuG the beamlets are refocused at the intermediate grids. In SINGAP, low-divergence beamlets at the exit of the 1 MV accelerator are obtained by providing *large diameter*, *convergent* pre-accelerated beamlets (fig. 2a).
3) Repulsion between beam groups due to their space charge.

In MAMuG, effects 1) and 3) are significantly mitigated by the presence of the intermediate grids. In SINGAP, the design geometry must counteract these effects. The beamlets must come out of the post-accelerator with low divergence and in the horizontal direction all beamlets must point to the middle of the RID exit apertures (located 7.1 metres downstream) [3]. The correct steering in SINGAP is largely provided by the electrode shapes.

Permanent magnets are embedded in the extraction and pre-acceleration grids to suppress electrons. The magnets introduce deflections of the D^- beams that must be kept small and in the vertical direction in order to avoid any adverse effect in the critical horizontal direction.

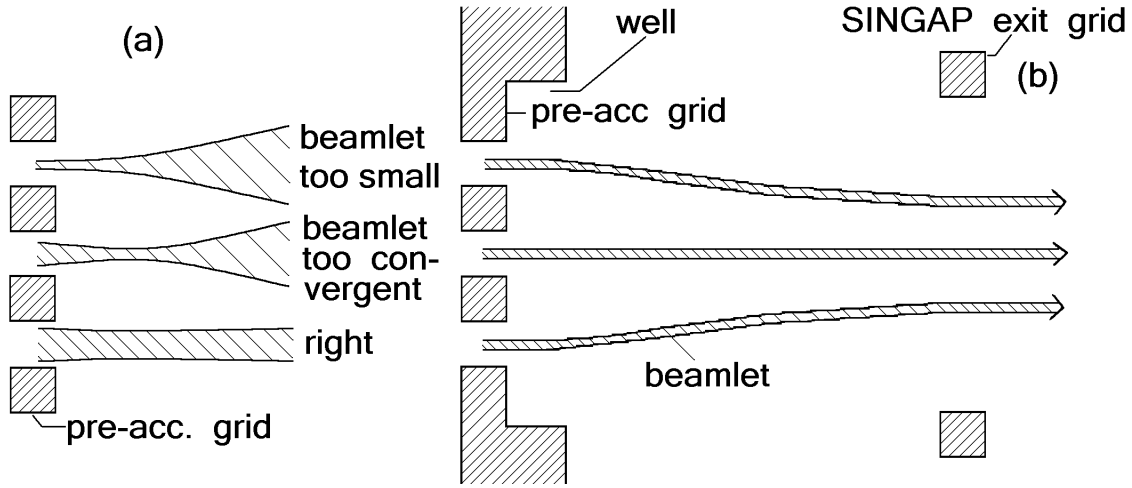

Figure 2: *The SINGAP physics principle:*
(a) beamlet properties
(b) action of a kerb or well.

3. Pre-accelerator

The task of the pre-accelerator is to provide the 1280 pre-accelerated beamlets with a beam optics that allows the SINGAP post-acceleration stage to produce low divergence, well directed beams. This requirement imposes the *large diameter*, *convergent* beamlets to be produced by it. Electrons must be almost completely suppressed to avoid their acceleration to 1 MeV. The beam optics is created by the electrode shapes and their electrostatic potentials. Electrons are suppressed by magnets embedded in the grid. It was found that the magnets do not affect the beamlet convergence but they do influence their direction. Care was taken to choose a configuration with low beam deflection and high electron suppression; all beam deflection is arranged to be in the vertical direction which is much less critical for beam transmission than the horizontal direction.

3.1 electrostatic configuration

To model the pre-accelerator, the 2-D SLACCAD code (Paméla [4]) has been used. Considering the literature, this code appears similar to IGUN (see e.g. Becker [5]). Both codes have been developed independently from the earlier electron gun code SLAC by Hermannsfeld [6]. While using SLACCAD, the module for electron extraction was not used because (1) in any usable negative ion system for ITER the space charge contribution from the electrons must be small and (2) there are a few problems in using this module. The module for stripping losses was used throughout. In the simulations, it was possible to produce 40 keV beamlets with a radius of 5.7 mm that leave the pre-accelerator with a convergence of 1.3° (23 mrad). The simulation result is in figure 3.

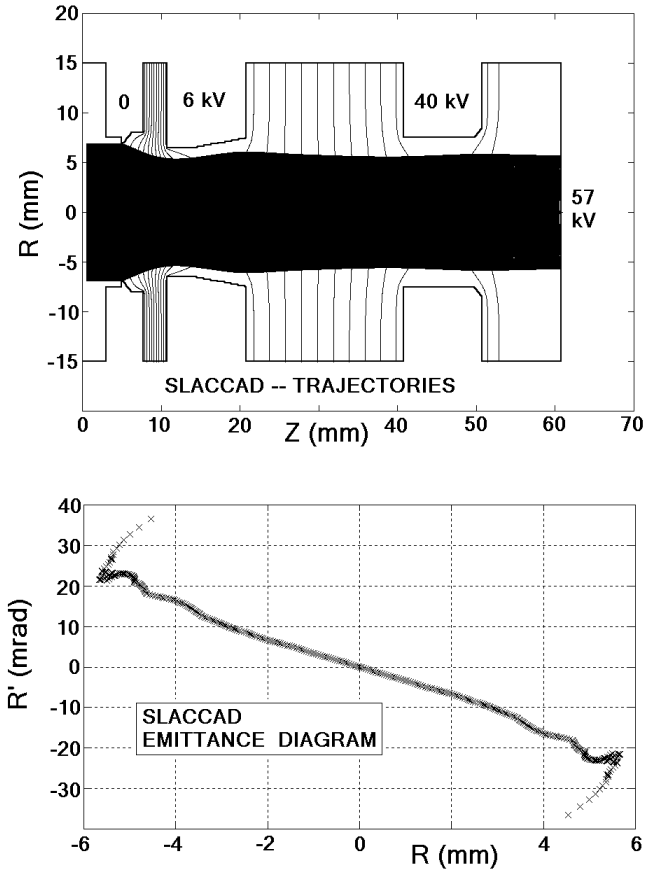

Figure 3: *Optics of the ITER SINGAP pre-accelerator for D^- calculated by SLACCAD. The current leaving the plasma grid aperture is 40 mA, which corresponds to 26 mA/cm^2 D^-. Stripping losses are included in the calculation.*

To complement the SLACCAD simulations, the 2-D code PBGUNS by Boers [7] has been used. In contrast to SLACCAD it is capable of simulating negative ion extraction from a plasma source by including the presence of positive ions, negative ions and electrons, each with their Boltzmann temperature distributions. The three species are simultaneously injected with a few eV energy at Z=0, moving downstream (Z>0) with the appropriate starting velocity set by the injection energy and the zero total space charge requirement at Z=0. The knife-edge of the plasma grid is set at Z=1 mm. For Z>0 Poisson's equation is solved and the potentials, particle densities and velocities (which influence each other strongly) are calculated. Neither code takes

account of the transverse magnetic (filter) field in the plasma in front of the plasma grid, which is present in most negative ion sources.

Testing PBGUNS in a positive ion configuration confirmed the earlier SLACCAD results. Running PBGUNS in negative ion mode revealed several differences; generally the plasma boundary is calculated flatter and more downstream by PBGUNS which causes a wider beam through the grid system. Retaining the present pre-accelerator for ITER requires an increase of the extraction voltage from 6 to 7 kV. In this way it will produce 40 keV pre-accelerated beamlets with a radius of 6.5 mm that leave the pre-accelerator with a convergence of 1.4° (25 mrad). This result (fig. 4) is, in fact, more suitable for the SINGAP optics than the SLACCAD result.

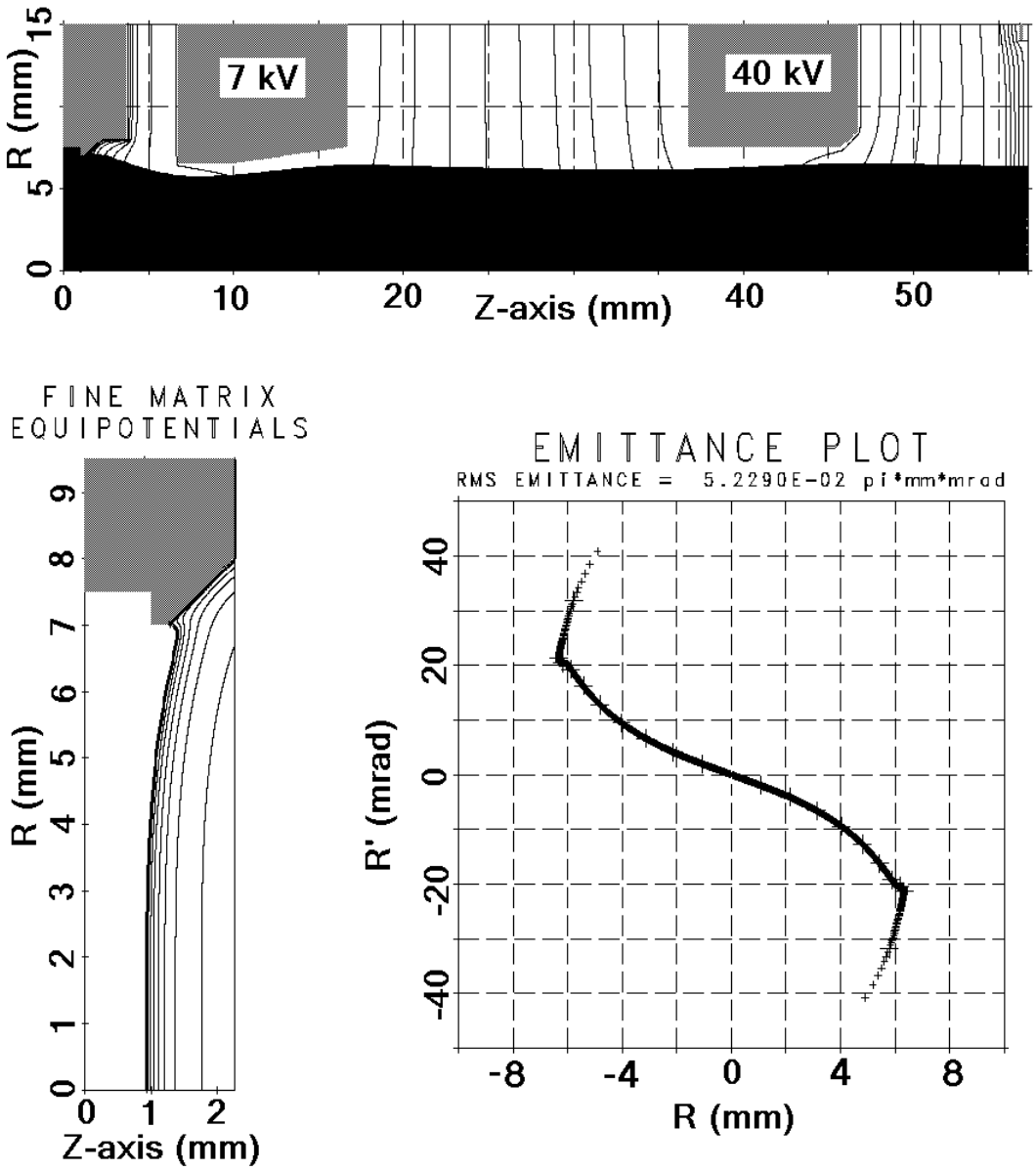

Figure 4: *Simulation of the ITER SINGAP pre-accelerator by PBGUNS with a 7 kV extraction voltage. The top picture shows the trajectories, the bottom left picture the equipotentials near the plasma boundary and the bottom right picture the emittance diagram 1 cm downstream of the pre-accelerator. Stripping losses are included by means of a 15% linear loss between Z=0 and Z=57 mm.*

3.2 magnetic configuration

Commercial Sm-Co permanent magnets with a surface strength of 0.96 Tesla are embedded in the extraction and pre-acceleration grids to deflect electrons onto the front surface of the grids. The magnets also affect the beam direction. To keep the deflection small, the North-South (NS) axis is parallel or antiparallel to the beam direction. Any deflection encountered on the upstream side of a grid will be partially compensated by a deflection in the opposite direction on the downstream side of the grid (because the ion energies are different on the two sides, the compensation is only partial). To further reduce the deflection, the magnets in the pre-acceleration grid are arranged in the opposite direction to those in the extraction grid.

The electron suppression magnetic fields are arranged in the horizontal direction in order not to have any influence on the critical horizontal beam direction. This implies that their fields are either added to, or subtracted from, the unidirectional filter field from the beam source. In simulating the beam deflection, two cases have to be considered as the suppression field direction in horizontally neighbouring apertures is opposite. The layout of the extraction and pre-acceleration grids is in figure 5.

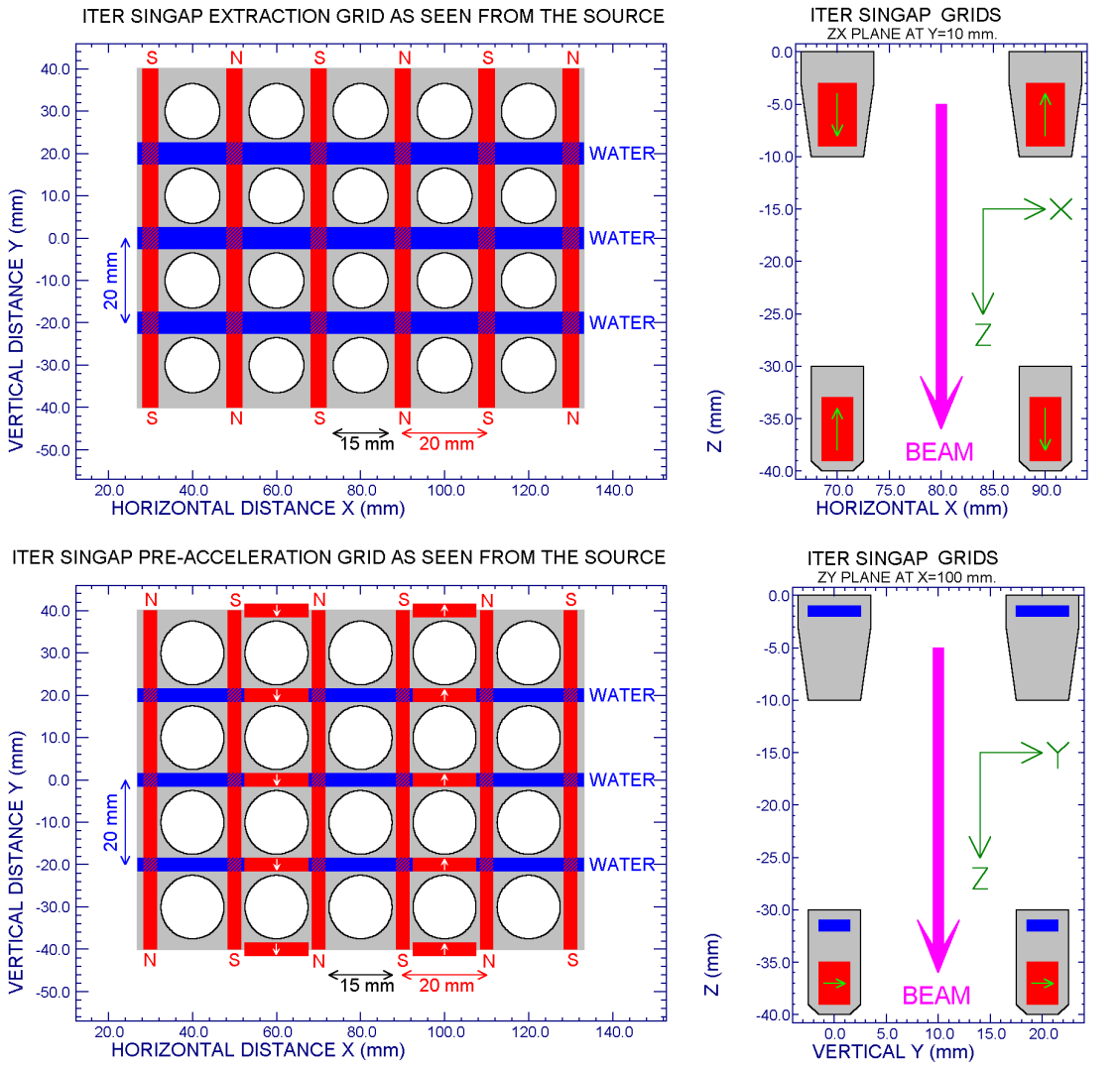

Figure 5: *Partial view of the SINGAP extraction and pre-acceleration grids. The two pictures on the left show the view from the source. Cooling channels and embedded magnets are shown. The two pictures on the right show a cut through the grids (top right: the ZX plane; bottom right the ZY plane).The direction of the magnetisation is indicated by arrows or with N and S where the view is on a pole.*

The electric fields have been calculated by SLACCAD [6] and by PBGUNS [7]. The 3D magnetic field map by the permanent magnets has been calculated with the CIRIC code (Ciric [8]). The magnetic field calculations by this code have been verified (by us) to accurately predict experimentally measured magnetic fields.

Included in the pre-acceleration grid are two columns of permanent magnets, referred to as *steering magnets*, that push beamlet columns 2 and 4 of each beam group closer to the axis. The steering magnets provide a 2 mrad correction on the horizontal optics of the 1 MeV post-accelerated D^- beam. Because the steering field is an order of magnitude smaller in the adjacent columns, the beamlets from columns 1, 3 and 5 in each beam group are hardly affected.

The electron leakage through the grids and the deflection of the ion beams has been calculated with an in-house developed particle trajectory code called TRACK. It tracks the particles through the electromagnetic fields in the pre-accelerator. Its accuracy is difficult to verify experimentally, but the positions of melt marks in several overheated extraction grids correspond quite well to the positions calculated by TRACK. A model for secondary emission was taken from the ELSTOP code by Simonin [9] and implemented in TRACK. Generally, an electron hitting a material surface has a chance of around 40% of being re-emitted again and this effect makes it possible for electrons to leak through the apertures, even in the presence of magnetic fields.

Figure 6 gives an example of electron and deuterium trajectories calculated by TRACK. Although figure 6 shows only 100 particles for clarity, TRACK calculations have been performed with 1 million electrons and 1 million D^- ions. The transmission of electrons through the extraction grid is around 4%. The transmission of electrons through the combined extraction and pre-acceleration grids is around 0.02%. The deuterium beams are not deflected in the horizontal direction, but in the vertical direction the deflection is +0.9 mrad for apertures where filter and suppression fields are additive; -4.7 mrad where these fields are subtractive. For H^- beams the figures are +0.9 mrad and -6.5 mrad, respectively. All values for beam deflection quoted have been evaluated 3 cm downstream of the 40 kV pre-acceleration grid, where the local potential is around 100 kV. After post-acceleration, these values for beam deflection will have been reduced by a factor of 3.

TRACK also calculates the electron power density profiles on the extraction grid. These are very peaked (fig. 7): power is expected to land either above or below the aperture, depending on the direction of the filter field and the suppression field. No overlay of the power from neighbouring apertures occurs, as is the case with the MAMuG reference design. Calculated power density is up to 1.0 kW/cm^2 on the surface of the extraction grid, but this drops to 600 W/cm^2 when evaluated over 1 mm^2 sections.

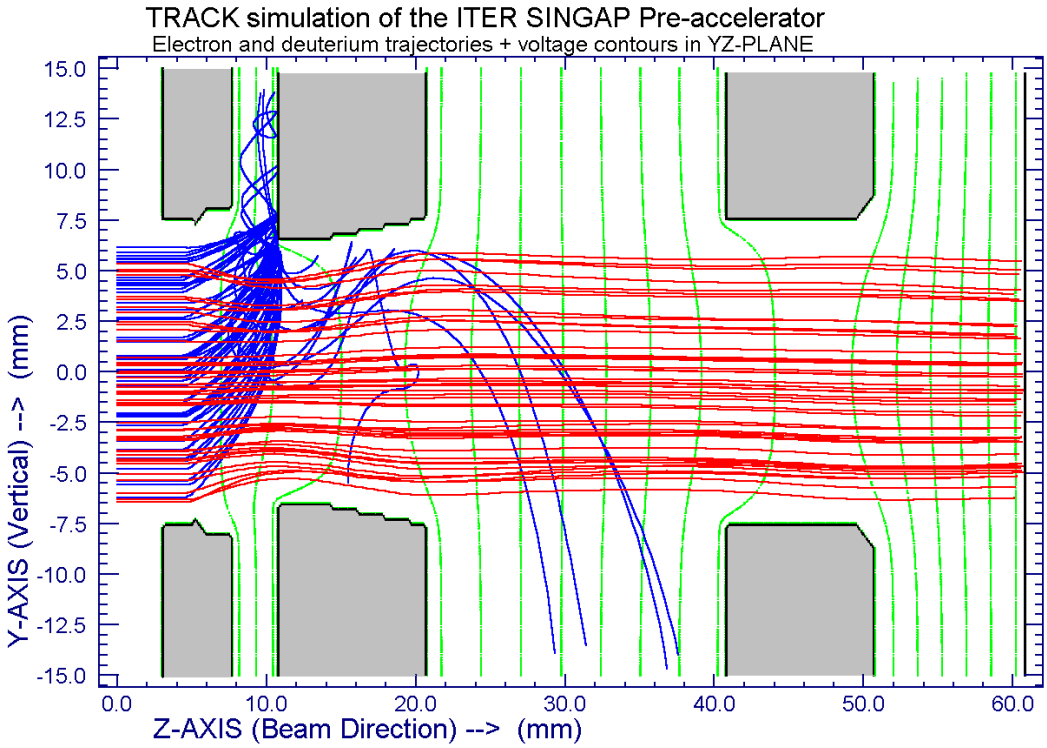

Figure 6: *50 Electron and 50 deuterium trajectories in the proposed ITER SINGAP pre-accelerator. Equipotential lines are also indicated. The equipotentials in the extraction gap are drawn at intervals twice as short as in the rest of the plot.*

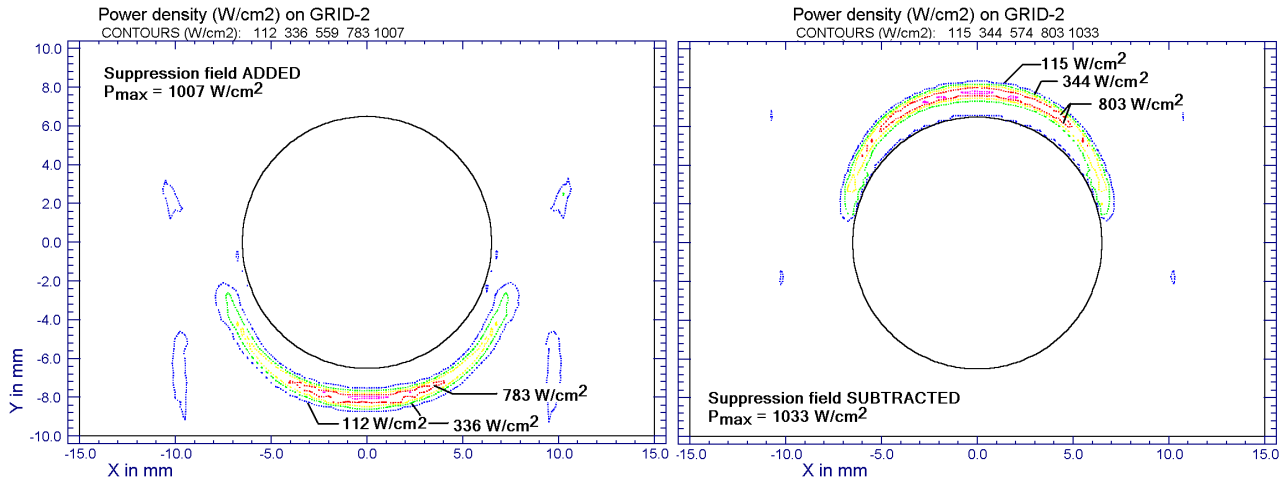

Figure 7: *Power density on the extraction grid by 26 mA/cm^2 co-extracted electrons. The electron suppression field either adds to the filter field from the source (left picture) or subtracts from it (right picture). Because the two apertures shown are horizontal neighbours, the power density profiles are not close to overlapping.*

4. SINGAP post-accelerator geometry

The pre-accelerated beamlets calculated by SLAC serve as input to the calculation of the post-accelerator. The SINGAP starting condition is determined by the ITER type segmented pre-accelerator. Thus one has sixteen 5x16 arrays of pre-accelerated beamlets, spaced 20 mm apart. In contrast to MAMuG, the spacing between apertures is the same in the horizontal as in the vertical direction.

As said in the introduction, our previous work [2] had to limit its considerations to ¼ of a beam group. The symmetry applied is equivalent to assuming an infinite number of beam groups. In the present work, a ¼ section of the *entire* problem is modelled, extending along the beam path from pre-acceleration grid to neutraliser. The modelling was done with the space charge module SCALA from the 3D electromagnetic software suite OPERA-3D by Vector Fields Ltd. [10]. The size of the hexahedral finite elements used was typically 10x10x10 mm^3 (670,000 elements in the model). A few cases have also been run at a reduced element size for which around 2 million elements had been used.

The extended modelling showed that the beam steering of the outer beam groups was not correct. The reasons were mainly geometrical in nature and will be described in the following paragraphs. The following changes to the SINGAP design from our earlier work [2] have been adopted:

1. "kerbs" on the pre-acceleration grid replaced with similar sized "wells".
2. "kerbs" have been added to the post-acceleration SINGAP grid.
3. The very large aperture sizes in the SINGAP grid have been slightly reduced.
4. The SINGAP grid is slightly "V-shaped" in the vertical direction.
5. The (intended) consequence of the above changes is that the substantial aperture offsets in the old design could be reduced to almost zero.

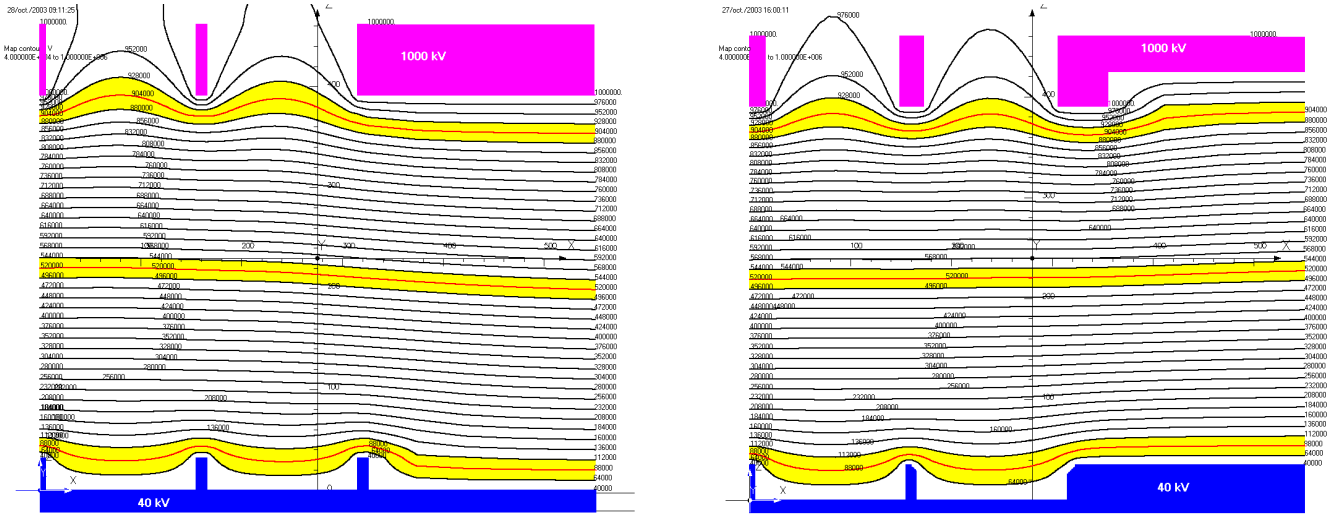

Figure 8: *Changing from "kerbs" to "wells" in the SINGAP accelerator. Both pictures represent a cross-section of SINGAP 197 mm above the midplane of the 16 beam groups; the beam direction is from bottom to top. In the left picture, kerbs are "bolted" on the 40 kV pre-acceleration grid. In the right picture, equivalent wells are "sunk" in a thick pre-acceleration grid. The minimum distance between material surfaces is in both cases 350 mm. In the left picture, the equipotential lines are defocusing away from the pre-acceleration grid. In the right picture this is not the case. Kerbs on the 1000 kV post-acceleration grid provide an additional focussing force towards the centre of the 16 beam groups. The effect of the new geometry can clearly be seen from the yellow zones, which represent the same potentials.*

In the new model, using the old geometry from our earlier work [2], the beams show an outward deflection, particularly the outer beam groups. This is even true in the absence of space charge. The deflection appears to be due to the fact that the SINGAP kerbs from ref. [2] were assumed to be bolted on the grid. This means that they were "sticking out" and the deformation in potential caused the beams to be deflected outwards. Arranging for a thick pre-acceleration grid into which the beam groups are sunk (so that the particles still feel the focussing influence of the nearby walls) largely corrected the problem. The situation is illustrated in figure 8. The left picture illustrates the situation from ref. 2. The right picture shows the new version of SINGAP.

The kerbs bolted on to the pre-acceleration grid (left picture) are meant to focus all the beamlets within one beam group. The consequence of their presence is that "far" from the grid the potential steers entire beam groups away from each other. This already occurs where the local electric potential exceeds 200 kV. In the new situation (right picture) the beamlets inside one group remain focussed but now the "far" away potential steers the entire beam groups towards each other.

It was considered useful to replace aperture offset steering by an alternative way of providing the correct beam alignment. In this way, aperture offset steering by changing the vertical position of the grounded SINGAP grid can be used to steer the beams between "on axis heating" and "off-axis heating" directions.

It was attempted to provide the steering by making the pre-acceleration grid "V-shaped" in either one or even two dimensions. Mini-kerbs attached to the wells had also been tried. We found in the end that the solution had to be very complicated. A further disadvantage is that making the pre-acceleration grid "V-shaped" decreases the distance between material surfaces, necessitating an increase in the gap width, which is not good for beamlet optics. The idea of shaping the pre-acceleration grid was therefore abandoned.

Making the post-acceleration grid "V-shaped" in the vertical direction provides the desired vertical steering without necessitating further complications.

Putting "kerbs" on the inside of the SINGAP post-acceleration grid provides horizontal steering of the beam groups towards the axis (the opposite as from kerbs on the pre-acceleration grid). The kerbs provide the horizontal steering and some vertical steering. The latter is taken into account when the amount of "V-shape" is determined. The kerbs had to be chosen 35 mm high to provide the desired horizontal steering. A range of kerb widths is possible. The choice of 25 mm wide was adopted because that case led to the simplest shape of the pre-acceleration grid. The pre-acceleration grid is completely flat, apart from the wells themselves.

Only a very slight horizontal aperture offset is needed in order to provide the finishing touch to the beam alignment. The horizontal inner apertures are 2 mm further out (i.e.: they are centred around X=±82 mm) and the horizontal outer apertures are 1 mm further in (i.e.: centred around X=±239 mm).

The final geometry arrived at is in figures 9 and 10. Figure 9 gives the geometry in a horizontal section at a vertical height of 207 mm. This is not exactly through the middle of a beam group (which is at 197 mm or at 591 mm) in order to allow the individual apertures in the pre-acceleration grid to be visible in the picture. The drawings stop at 1000 mm for clarity. The proposed support flanges for ITER extend further than this; the shape of the grid must be continued in the support flanges.

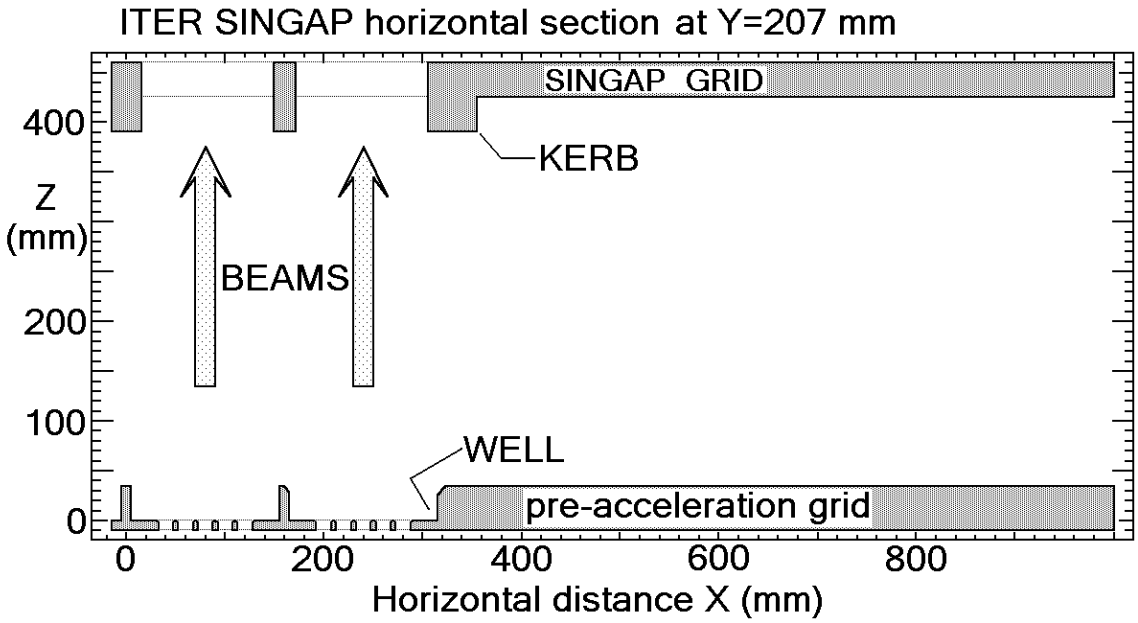

Figure 9: *Horizontal cross-section through the SINGAP post-accelerator taken at Y=207 mm above the accelerator midplane.*

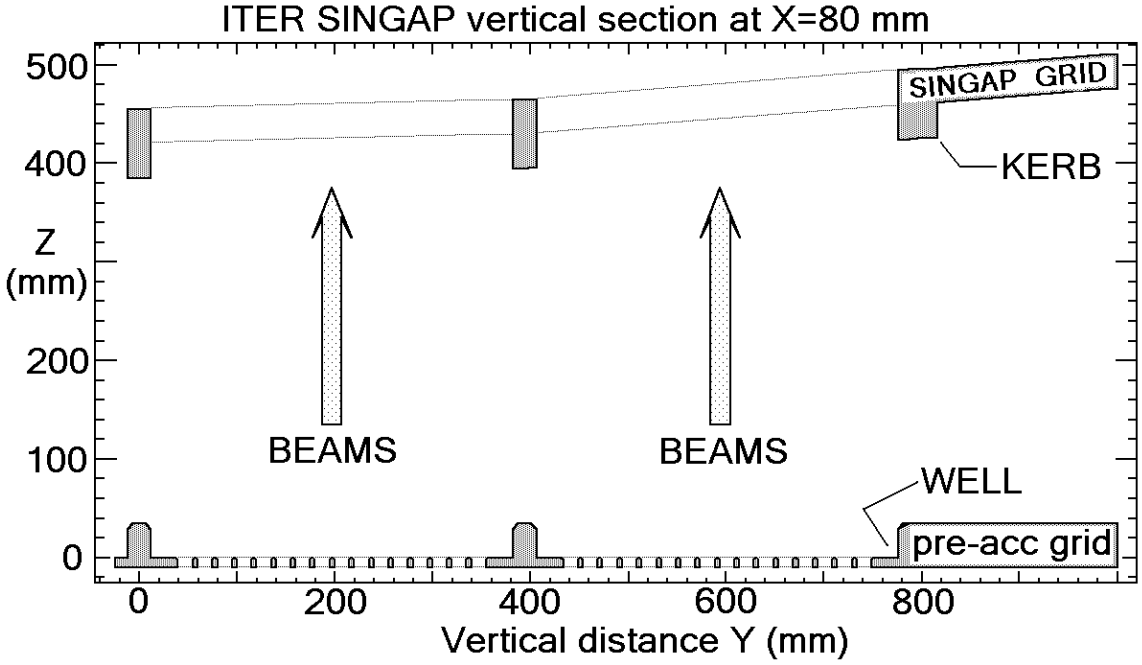

Figure 10: *Vertical cross-section through the upper half of the SINGAP post-accelerator taken at X=80 mm from the vertical accelerator midplane. The vertical slope ¶Z/¶Y of the SINGAP grid is 10/394 (1.5°) for the inner beam groups (úYê<394 mm) and 30/394 (4.4°) for the outer beam groups and beyond.*

The geometry in figures 9 and 10 is as modelled with the Vector Fields code [10]. To facilitate the modelling the geometry is entered with sharp edges. It is envisaged to round all the sharp corners. In the model the maximum field strength, calculated with 3.3x5x10 mm^3 finite elements and sharp edges, is 57 kV/cm.

5. Emittance

The simulations of the SINGAP post-accelerator were performed by representing each beamlet with a single ray in SCALA. Care was taken that the starting position of each ray corresponds to the exact middle of an emitting finite element. If this is not done, the ray would be deflected by its own space charge. In this way the *direction* of each individual beamlet in the accelerator is modelled. Interaction between the individual beamlets and between beam groups is included as SCALA takes it all into account.

Once the charged particle beam is beyond the electric fields from the accelerator, its space charge will be compensated by positive ions formed in reactions between the negative ion beams and the background gas. Because the exit apertures of the SINGAP exit grid are very wide, the electric field from the accelerator penetrates beyond the exit grid and it is not clear where exactly space charge compensation starts. Typically, one expects this to be of the order of the aperture width downstream of the grid. The post-accelerator kerbs are chosen to be 70 mm long in the beam direction in order to form a maximum in the electric potential near the grid. This is meant to prevent positive ions from escaping into the accelerator and in this way stimulate space charge compensation. The maximum potential occurs at 110 mm downstream of the front-end of the kerbs (40 mm downstream of the backside of the SINGAP grid) and it has been assumed that compensation of the beam space charge starts here. Therefore, all emittance diagrams are calculated 40 mm beyond the downstream side of the post-acceleration grid kerbs. It is assumed that the beam propagates linearly from that point onwards. A picture of the potentials on lines going through the middle of the beam groups is in figure 11.

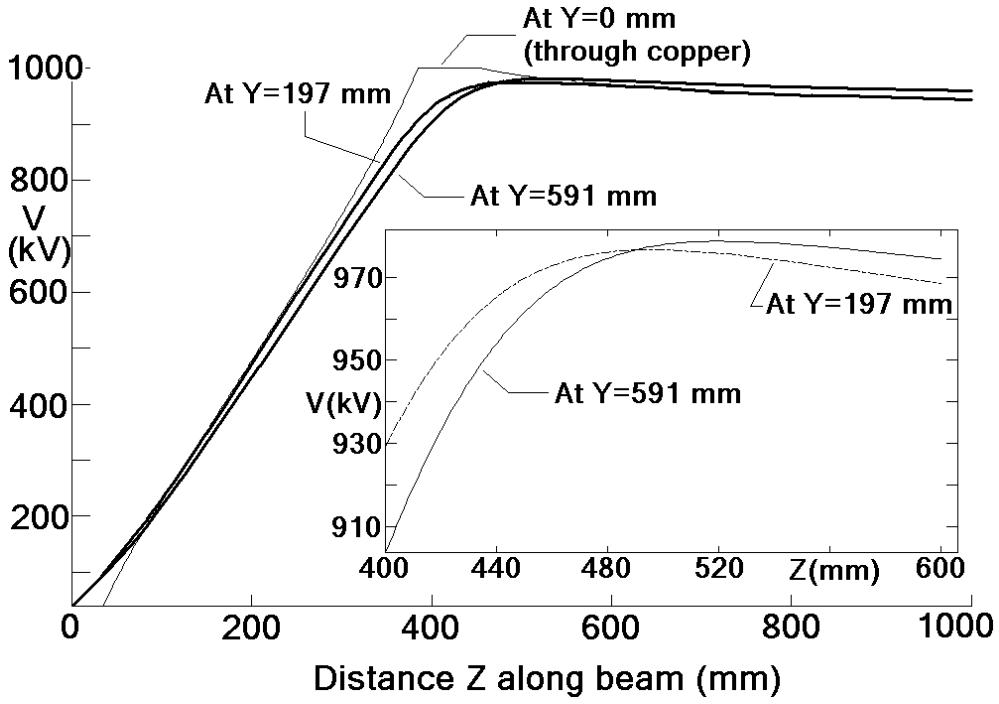

Figure 11: *Electric potential on two lines going through the middle of the beam groups at Y=191 and Y=591 mm. The groups at Y=591 mm see a lower electric field over a longer distance as the SINGAP grid is further away (figure 10). A thin line through Y=0 is also plotted; it has plateaus because it goes through metal surfaces. The inset shows the detail around the maximum in the electric potential.*

The divergence of the individual beamlets cannot be calculated with this model as the size of the finite elements is larger than the radius of the beamlets. One can therefore not expect to generate electric fields on this mesh that represent space charge repulsion inside each individual beamlet.

Although the divergence of the individual beamlets cannot be modelled inside the big model which includes the full geometry, it can be modelled in an approximate fashion in two different ways.

- **Semi-analytically.** The starting conditions (radius, convergence, energy, current, mass) at Z=0 can be used to calculate the same parameters slightly downstream in a homogeneous electric field; the new values then serve again as starting parameters for another step. The divergence calculated 40 mm beyond the downstream side of the SINGAP grid is 2.3 mrad. This procedure had been extremely valuable in establishing that it was large radius, converging beamlets that were needed for SINGAP to produce low emittance beams.
- **Numerically, under simplified assumptions.** The element size from our earlier work [2] that modelled only ¼ of a beam group was 1.8x2.6x14 mm^2 and the calculated divergence of *columns* of individual beamlets was around 4 mrad (a column is 8 beamlets and the emittance diagram for the column is a convolution of direction and divergence for the 8 beamlets). We have updated this ¼ beam group model to the present geometry and thanks to advances in information technology since the year 2001, we could rerun it on a 1x1x10 mm^3 finite element mesh (the long 10 mm dimension is parallel to the nominal beam direction). Therefore, contrary to the semi-analytical model described above, distorting effects due to the presence of the kerbs and wells are taken into account. The simulation represented each beamlet by 1000 rays. Using colour to distinguish between different beamlets from the same column, we could isolate the divergence while deliberately ignoring directional effects which are properly included in the main model. The individual beamlet divergence simulated this way came out to be around 3.0 mrad (inside a range from 2.0 to 3.5 mrad).

To obtain a full description of the SINGAP beam optics, the 1280 positions and *directions* are taken from the large model. Then, each of the 1280 beamlets is assumed to have a divergence of 3 mrad (or any larger value if one wants to be pessimistic). This information is then used in a transmission code to calculate the power transmitted to ITER by SINGAP.

The emittance diagram for the adopted SINGAP geometry in figure 10 is in figure 12. Each point in the diagram represents the position and direction of one individual beamlet. The data is taken in a plane parallel to the SINGAP grid, 40 mm to the downstream side.

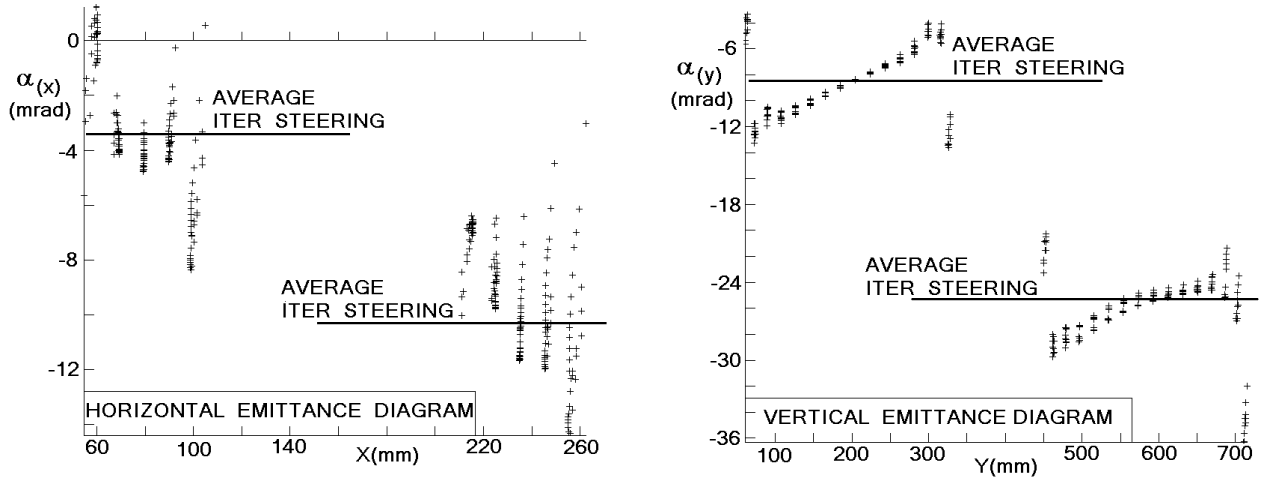

Figure 12: *Emittance diagrams taken 40 mm downstream of the proposed SINGAP grid in figure 10. The diagrams represent ¼ of the system; the rest (negative values for X and/or Y) is implied by symmetry. Each point represents position and direction of 1 beamlet. More detailed calculations on a small subsection of the system indicate that each point has a divergence of around 3 mrad. The required beam group steering for ITER is indicated by the horizontal lines labelled "AVERAGE ITER STEERING".*

6. Beam transmission

The transmission through the ITER beamline has been calculated using an in-house developed code, TRANSMIT, that models the beam as the sum of the individual beamlets. TRANSMIT considers a test plane, a plane perpendicular to the beam direction at the exit of the neutral beam duct, in the ITER case 23.4 metres from the grounded grid. The test plane is subdivided in small rectangles, 5mm by 5mm in our case. For each small rectangle, it is determined which of the 1280 beamlets (each with their own position, steering and Gaussian divergence) is "seen" by that rectangle and which of the 1280 is blocked by one of the scrapers defined in the program. If power is "seen" by a rectangle, its magnitude depends on the Gaussian parameters (direction, divergence and beamlet starting radius (assumed to be 4 mm)) for each individual beamlet. Provided the test plane is large enough to intercept 100% of the unscraped beam and the "scrapers" are arranged in an upstream to downstream order, TRANSMIT provides the power intercepted by each scraper. These "scrapers" are chosen to have the same beam limiting geometry of the ITER beamline components such as the Neutraliser, RID, etc.

It is necessary to take account of the fact that the calculated emittance is only as good as the code that was used for the calculations and the input data. The codes used (SLACCAD, PBGUNS and SCALA) do not take into account all the physics of negative ion extraction and acceleration, or the engineering of the ion source and accelerator. Some aspects that affect the real emittance are:

- The temperature of the extracted ions is finite, not zero as assumed in SLACCAD.
- The actual system will have mechanical inaccuracies that are not in the codes.
- The alignment of the apertures in the different grids will not be perfect, as assumed in the codes. Misalignment will occur from mechanical imperfections and thermal distortion and expansion of the grids.
- The flux of D^-/H^- to the plasma grid from the ion source will not be perfectly uniform across the aperture array on the plasma grid (as assumed in the code) - there may be both spatial and temporal variations.
- The plasma meniscus (from which the negative ions are emitted into the extractor) may not be exactly as in the codes since they do not contain all the physics that might affect that boundary, such as the effect of the magnetic filter field in the ion source and its variation across the plasma grid.
- The variation in stripping across the accelerator due to the lateral pressure gradient changes the effect of space charge at different lateral positions. This is not in the codes.

Because the codes do not completely take into account all the effects affecting the emittance, it is usual that the measured emittance is worse than the calculated one. Thus when calculating the power deposition in the beamline it is necessary to take this into account. As we are ignorant of the actual beam emittance we will have, we have adopted an assumption that we refer to as "realistic beams". "Realistic beams" assumes that on top of the calculated emittance diagram and individual beamlet divergence:

- An extra divergence of 2 mrad is added to the calculated beamlet divergence,
- A random extra divergence between 0 and 1 mrad is added to the beamlet divergence,
- A random direction (in X and Y) between –1 and +1 mrad is added to the direction of each beamlet.

"Realistic beams" do not assume the presence of a halo as was done for the ITER design, which assumed that 15% of the beam power is in a halo with 15 mrad divergence. The transmission of a 15 mrad halo through the ITER beamline is 43%, almost independent of any other parameters. The reason for the constant transmission is that the beam footprint at the exit of the residual ion dump is much wider than the slits of that component; therefore the exact direction of the beamlet doesn't matter anymore.

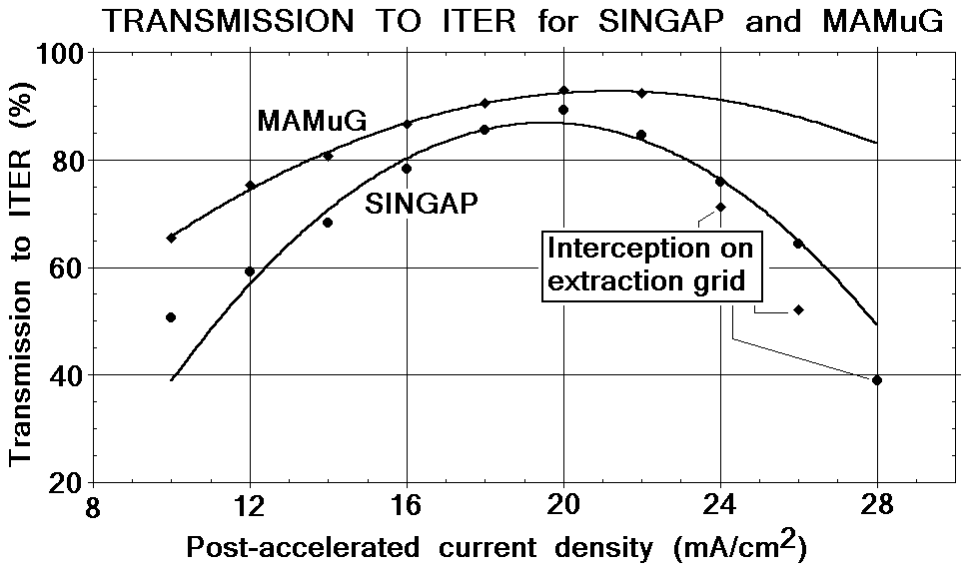

Figure 13: *The transmission to ITER by SINGAP and MAMuG for 1 MeV D^- beams at different post-accelerated current density. At high current density interception on the extraction grid occurs, sooner for MAMuG than for SINGAP. At low current density, the transmission for MAMuG is better than for SINGAP because in the SINGAP case the direction of the individual beamlets changes. The curves are quadratic fits through the main data to guide the eye.*

The "realistic beams" assumption, without including a halo has been applied to the reference MAMuG design and the present SINGAP design. The calculated beamlet divergence for both cases is around 3 mrad. The calculated transmission is:

- for MAMuG: 88.1%
- for SINGAP: 85.5%

Using identical assumptions, SINGAP has a beam transmission that is 2.6% less than MAMuG.

Perveance curves (fig. 13) have been calculated by varying the post-accelerated D^- current density (j=10-28 mA/cm^2) at 1 MeV. For MAMuG, the code SLACCAD has been used to calculate the 1 MeV beam optics. For SINGAP, SLACCAD was used to calculate the pre-accelerated beam optics and SCALA was used to calculate the post-accelerated beamlet directions (the divergence of which was estimated with the semi-analytical calculation described in section 5). Using this procedure, the best beamlet divergence is calculated to be 2.3 mrad, both for MAMuG and SINGAP. Therefore, the maximum transmission in figure 13 is slightly higher than mentioned above.

In the case of SINGAP the extraction and pre-acceleration grids intercept part of the beam for j>26 mA/cm^2. For MAMuG interception on the extraction grid occurs already for j>22 mA/cm^2. Interception on the extraction grid occurs sooner for MAMuG than for SINGAP because the MAMuG extraction grid is thicker and the diameter of the apertures inside is smaller. It should also be noted that the calculation of the perveance curves did not include any magnetic fields. Inclusion of magnetic fields leads to the beamlets being deflected and hitting extraction and pre-acceleration grids sooner than indicated in figure 13. To calculate the transmission, the post-accelerated beamlet parameters have been made 'realistic' in the same way as described above but no halo is included.

One should also realise that as the source will not be perfectly uniform and there will be ripple on the electrode voltages, the actual transmission to ITER will be some kind of average over a range of current densities, therefore always lower than the maximum value in fig. 13.

7. Electron deposition

The deuterium pressure inside the SINGAP main acceleration gap is expected to be around 0.03 Pa (Krylov *et al.* [11]). This causes stripping reactions of the partially accelerated negative ions inside the main acceleration gap. These electrons are then accelerated to an energy of up to 960 keV, depending on their position of birth. They subsequently escape from the accelerator through the very large apertures and are deposited on or near the neutraliser. The magnetic filter from the source induces a vertical deflection and the residual vertical stray field from the ITER tokamak induces a horizontal deflection. To avoid hitting the cryo pumps with electron beams it is essential that the magnetic filter is arranged in such a way that the electron beam is deflected downward.

The total power in stripped electrons is calculated to be 2.7 MW. This power needs to be properly dealt with downstream of the accelerator. Moreover, the electrons produce X-rays when they impact on metal surfaces. These X-rays can heat the cryo pumps internally. Also scattered electrons can heat the cryo pumps. The problem (electrons and X-rays) is being studied by M. Kovari [12].

To calculate the deposition of electrons, we used the magnetic configuration from the latest proposal by the Japanese Home Team [13]. The original proposal was to provide the necessary filter field to the KAMABOKO negative ion source by passing a current of 8 kA through the plasma grid (this type of filter is called PG filter). This solution leads to high magnetic fields in the accelerator, which was deemed unacceptable. The present configuration uses a 4 kA PG filter, supplemented by an arrangement of permanent magnets that adds to the PG field inside the source, but subtracts from it outside. It is this magnetic configuration that was used in the simulations. The field is plotted in figure 14.

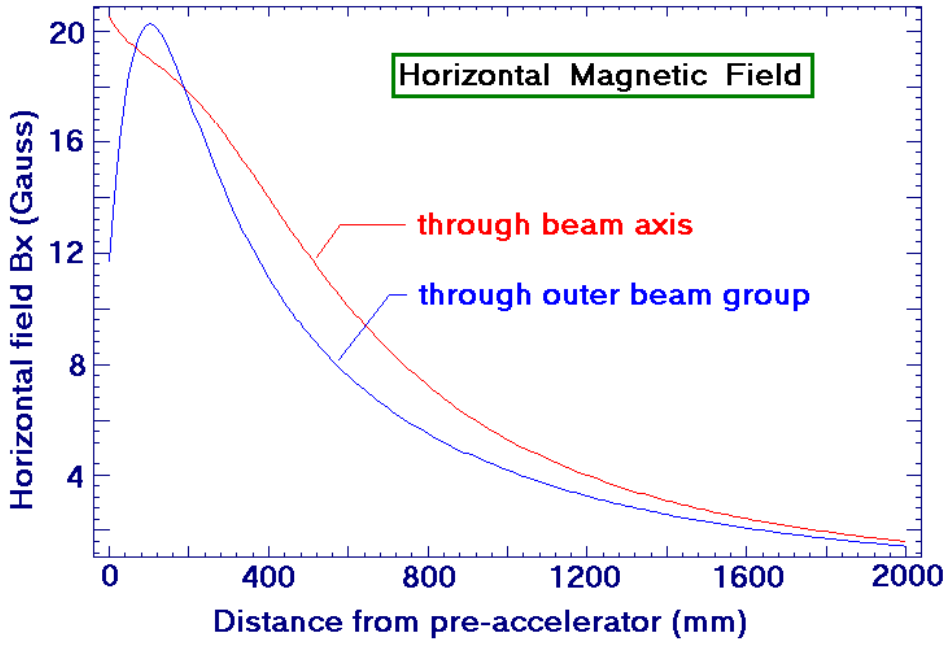

Figure 14: *Calculated horizontal magnetic field (in Gauss) between the pre-accelerator and the neutraliser. The red line gives the field on the symmetry axis of the system, the blue line through the outer beam group at (x,y,z)=(240,594,0) mm, where y is upwards and z is horizontally in the beam direction. The field in the neutraliser is less than 2 Gauss; the field in the post-accelerator is around 16 Gauss. The pre-acceleration grid is at z=0 mm, the neutraliser is at z=2000 mm.*

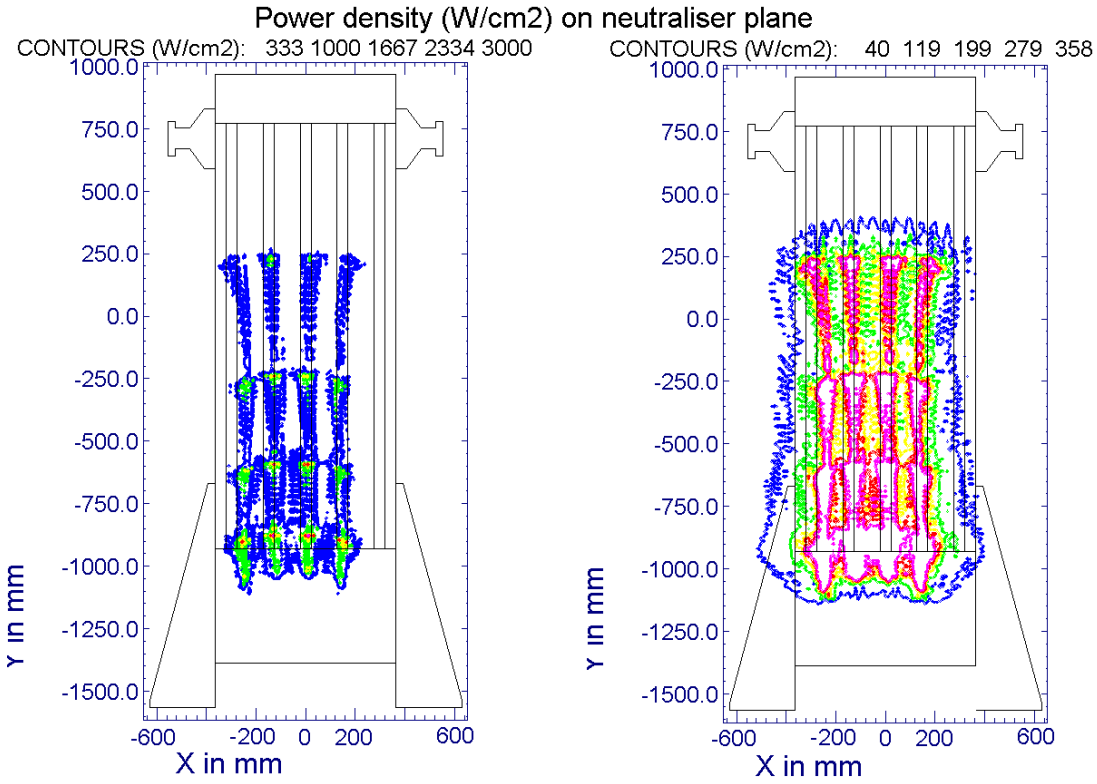

Figure 15: *Power density contours of electron power deposited on the neutraliser plane. Small local hot spots of 3.3 kW/cm^2 occur on the neutraliser leading elements. The right picture gives power density contours up to 390 W/cm^2.*

The magnetic field produced by the permanent magnets around the KAMABOKO source was calculated with the CIRIC code [8]. The contribution of a planar current flowing through the plasma grid was added numerically. In the DDD [3], it had been attempted to calculate the vertical stray field from ITER, taking the passive shielding and active compensation coils into account. As different codes obtained different results, we simply assumed the field to be a uniform 1 Gauss. TRACK was used to follow the trajectories of electrons created in the SINGAP accelerator on the deuterium trajectories. The calculations are relativistic, as the electrons are accelerated up to 1 MeV, well above their rest mass of 0.511 MeV.

Figure 15 gives the calculated electron power density on the neutraliser plane, located 2.0 m downstream of the pre-acceleration grid. The RFX team in Padova [14] is presently calculating whether the neutraliser leading elements can take the power.

8. First experiments and future developments

The SINGAP testbed in Cadarache has been described by Desgranges *et al.* [15]. Beam optics tests had been conducted satisfactorily on it, but the geometry was not ITER-relevant and also introduced rather large uncertainties in the interpretation of the results (de Esch *et al.* [16]). Therefore, a new prototype SINGAP accelerator is now being tested that closely resembles the accelerator outlined in this paper. Although only good for 100 mA D^-, it features exactly the same pre-accelerator but modified wells. The modification is necessary to accommodate the difference between 100 mA beams and 40 A beams. This accelerator is now being used to test the SINGAP design, especially the aspect of the large diameter converging beamlets. An experiment to test beam steering by anode aperture offset has also been conducted.

The experimental results from this programme are described by Svensson *et al.* [17]. It has been reported that the experimental aperture offset steering matches the calculated effect precisely. The divergence of individual beamlets has been estimated under the same perveance-match

conditions as the ITER SINGAP accelerator. It came out at 3.6 mrad horizontally and 5.2 mrad vertically. These values were arrived at after taking into account the diffusion of heat in the target. Such tests have been performed at 490 kV, 6.3 mA/cm^2 on target under pressure conditions ~40% higher than foreseen on ITER. In addition to the acceptable divergence of the main beamlet, a 30% halo has been observed.

It is planned to test the SINGAP accelerator in a 1 A testbed at JAERI in Japan. This is foreseen to take place in the near future.

Finally, a choice is to be made between SINGAP and MAMuG when the construction of the ITER neutral beam testbed is decided.

9. Conclusions

Increased computing power has revealed faults in the design of the SINGAP 1 MeV, 40 A, D^- accelerator for the ITER neutral beam injectors. The new design presented in this paper eliminates those faults and results in improved performance and larger safety margins, whilst maintaining the engineering simplicity of the previous design. In particular each of the 4 "sub-grids" that make up one grid are completely flat, all the apertures in the pre-accelerator are aligned, and the need to tilt the entire 26 tonne beam source to move the beam between on-axis and off-axis plasma heating is avoided.

- The extraction gap is reduced to 3 mm, which allows the use of a lower extraction voltage for the best optics at a given extracted current density. This minimises the power from the co-extracted electrons deposited on the extraction grid.
- The magnets incorporated in the extraction and pre-acceleration grids (for electron suppression) are oriented so as to deflect charged particles in the vertical direction, which avoids deflection of the negative ion beam in the critical horizontal direction. The deflection due to the magnets in the extraction grid is opposite to that from the magnets in the pre-acceleration grid, which minimises the vertical beam deflection, to a maximum of 1.6 mrad for 1 MeV D^-. This is sufficiently small that no correction by, for example, offset aperture steering is required.
- The pre-acceleration grid has been modified to incorporate 35 mm deep "wells", and the resulting electrostatic lens counteracts the interaction between beamlets.
- "Kerbs" mounted on the post acceleration grid modify the electric field distribution, which then provides the desired horizontal steering and some vertical steering. The required overall vertical steering is achieved by the aforementioned kerbs plus making the grid "V"-shaped in the vertical plane.
- The design allows aperture-offset steering (at the grounded grid) to be used to move the beam between on-axis and off-axis plasma heating, as required by ITER, which avoids the use of a tilting mechanism for the 26 tonne structure.
- The transmission to ITER is similar to that expected from the reference (MAMuG) accelerator design, 86%, compared to 88% for MAMuG.
- First experimental results indicate post-accelerated beamlets somewhat wider than the calculated 2.5 mrad.

Acknowledgement

The help and support by Dr. D. Ciric in making his magnetic field code available is highly appreciated.

References

[1] T. Inoue et al., Design of Neutral Beam System for ITER-FEAT, Fusion Engineering and Design **56**-**57**(2001)517.

[2] H.P.L. de Esch, R.S. Hemsworth and P. Massmann, SINGAP: The European concept for negative ion acceleration in the ITER neutral injectors, Rev. Sci. Inst. **73**(2002)1045.

[3] ITER DDD5.3 http://132.169.11.26/iter-doc/ddd/ddd53/ddd53_index.html

[4] J. Paméla, A model for negative ion extraction and comparison of negative ion optics calculations to experimental results, Rev. Sci. Inst. **62**(1991)1163
[5] R. Becker, New features in the Simulation of Ion Extraction with IGUN, EPAC 1998, Stockholm. Electronically published on http://www.JACoW.org/ Direct link: http://accelconf.web.cern.ch/AccelConf/e98/PAPERS/THP44G.PDF.
[6] W.B. Hermannsfeld, Electron Trajectory Program, SLAC report, Stanford Linear Accelerator Center, SLAC-226 (1979).
[7] J.E. Boers, PBGUNS manual, available through Thunderbird Simulations, 626 Bradfield Drive, Garland 75042-6005, Texas 75042-6005, USA. http://www.thunderbirdsimulations.com
[8] D. Ciric, private communication and support.
[9] A. Simonin, High Efficiency Trapping of Stray Electrons in Negative Ion Accelerators, 7th international symposium on Production and Neutralisation of Negative Ions and Beams *combined with* 6th European Workshop on Production and Application of Light Negative Ions, (Upton, NY, 1995). AIP Conference Proceedings 380, page 378, ISBN 1-56396-565-8, DOE CONF- 9510304, Editor K. Prelec, ©1996
[10] Vector Fields Ltd, 24 Bankside, Kidlington, Oxford OX5 1JE, UK. Tel: (+44)(0)1865 854999. http://www.vectorfields.co.uk
[11] A. Krylov and R.S. Hemsworth, *Gas flow and related beam losses in the ITER beam sources*, to be published in Fusion Engineering and Design.
[12] M. Kovari, private communication.
[13] M. Kashiwagi, private communication.
[14] Mauro Dalla Palma and Pier-Luigi Zaccaria, private communication.
[15] C. Desgranges, J. Bucalossi, M. Fumelli, R.S. Hemsworth, P. Massmann, J. Paméla and A. Simonin, *Results of the 1 MV SINGAP Experiment,* 8th Int. Symposium on the Production and Neutralization of Negative Ions and Beams, Giens (France), September 1997. AIP conference proceedings 439, page 187, ISBN 1-56396-737-5, ISSN 0094-243X, Editor C. Jacquot, ©1998.
[16] H.P.L. de Esch, D. Boilson, R.S. Hemsworth, P. Massmann and L. Svensson, *First Simulations of the Cadarache SINGAP Experiments,* 9th Int. Symposium on the Production and Neutralization of Negative Ions and Beams, Gif-sur-Yvette (France), May 2002. AIP conference proceedings 639, page 184, ISBN 0-7354-0094-6, ISSN 0094-243X, Editor M.P. Stockli, ©2002.
[17] L. Svensson, D. Boilson, H.P.L. de Esch, R.S. Hemsworth and A. Krylov, *Experimental results from the Cadarache 1 MV test bed with SINGAP accelerators*, this conference.